Design and Stability of an On-Orbit Attitude Control System Using Reaction Control Thrusters

Robert A. Hall[1]
CRM Solutions, Inc., Jacobs ESSSA Group, Huntsville Al, 35812

Steven Hough[2]
Dynamic Concepts, Inc., Jacobs ESSSA Group, Huntsville, AL, 35812

Carolina Orphee[3]
NASA Marshall Space Flight Center, Huntsville, AL, 35812

Keith Clements[4]
Engineering Research and Consulting, Inc., Jacobs ESSSA Group, Huntsville, AL, 35812

Basic principles for the design and stability of a spacecraft on-orbit attitude control system employing on-off Reaction Control System (RCS) thrusters are presented. Both vehicle dynamics and the control system actuators are inherently nonlinear, hence traditional linear control system design approaches are not directly applicable. This paper has two main aspects: It summarizes key RCS design principles from earlier NASA vehicles, notably the Space Shuttle and Space Station programs, and introduces advances in the linear modelling and analyses of a phase plane control system derived in the initial development of the NASA's next upper stage vehicle, the Exploration Upper Stage (EUS). Topics include thruster hardware specifications, phase plane design and stability, jet selection approaches, filter design metrics, and RCS rotational maneuver logic.

Nomenclature

J_1 = Principal Moment of Inertia about X axis (slug-ft^2)
J_2 = Principal Moment of Inertia about Y axis (slug-ft^2)
J_3 = Principal Moment of Inertia about Z axis (slug-ft^2)
$\hat{J}$ = Inertia Tensor (slug-ft^2)
ω_1 = Inertial body rate about X axis (rad/sec)
ω_2 = Inertial body rate about Y axis (rad/sec)
ω_3 = Inertial body rate about Z axis (rad/sec)
$\hat{\omega}$ = Body rate vector with respect to inertial frame (rad/sec)
T_{1ext} = External disturbance torque on X body axis (ft-lb)
T_{2ext} = External disturbance torque on Y body axis (ft-lb)
T_{3ext} = External disturbance torque on Z body axis (ft-lb)
$\hat{T}_{ext}$ = External disturbance torque vector in body axes (ft-lb)
$\hat{T}_C$ = Control torque vector in body axes (ft-lb)
u_1 = Control torque on X body axis (ft-lb)
u_2 = Control torque on Y body axis (ft-lb)
u_3 = Control torque on Z body axis (ft-lb)

[1]Technical Director for GN&C (Jacobs ESSSA Group); NASA MSFC Huntsville AL 35812: robert.a.hall@nasa.gov
[2]Aerospace Engineer (Jacobs ESSSA Group); NASA MSFC, Huntsville, AL 35812: steven.l.hough@nasa.gov
[3]Aerospace Engineer; NASA MSFC, Huntsville, AL 35812: m.carolina.orphee@nasa.gov
[4]Control Systems Analyst (Jacobs ESSSA Group); NASA MSFC, Huntsville, AL 35812: keith.r.clements@nasa.gov

Λ_{IB} = Quaternion from Inertial to Body Frame (unitless)
φ = Eigen angle from inertial frame to body frame (rad)
$\hat{a}$ = Eigen axis from inertial frame to body frame (unitless)
η = Scalar portion of quaternion Λ_{IB} (unitless)
$\hat{\varepsilon}$ = Vector portion of quaternion Λ_{IB} (unitless)
δ = Phase plane attitude deadband (rad)
δ_H = Phase plane attitude deadband hysteresis (rad)
RL = Phase plane rate limit (rad/sec)
τ = Rate gain representation for phase plane, $\tau = \delta / RL$ (sec)
Λ_e = Quaternion from current attitude to desired attitude (unitless)
ϕ_e = Eigenangle (or Euler angle) from current attitude to desired attitude (rad)
$\hat{a}_e$ = Eigen axis (or Euler axis) from current attitude to desired attitude (unitless)
ϕ_e = Attitude error (rad)
ω_e = Rate error (rad/sec)
ϕ = Vehicle attitude angle in single axis formulation (rad)
$\dot{\phi}$ = Vehicle attitude rate in single axis formulation (rad/s)
θ_r = Rigid body phase margin (deg)
a_c = Control acceleration (rad/sec^2)
$N(A)$ = Describing Function with input amplitude A (units vary)
Ψ = Current phase plane output command (unitless)
Ψ_c = Updated phase plane output command (unitless)
T_D = System latency (sec)
T_F = Allowable filter lag (sec)
Δ = Intermediate describing function variable (unitless)
λ = Intermediate describing function variable (unitless)
A_{jets} = Matrix whose columns are the jet acceleration vectors (deg/sec^2)
b = Column vector of commanded body rates (deg/sec)
x = Column vector of commanded jet on times (sec)
P = Cost function to minimize propellant to achieve a rate command (lbs)
c = Row vector of thruster flow rates for each thruster (lbs/sec)
ω_m = Desired maneuver rate magnitude (deg/sec)

I. Introduction

The use of on-off Reaction Control System (RCS) thrusters for on-orbit attitude control is a well-utilized and well-proven approach. The vehicle rigid body dynamics and the discontinuous on-off thrusters provide a nonlinear plant and nonlinear control system, however, making traditional linear design and analysis approaches generally unavailable. Advances in design and certification of thruster systems were made with the extensive use of RCS control in Space Shuttle and International Space Station (ISS) programs. In particular, advancements were made with the filter design and certification of RCS control in the presence of low frequency flex-body dynamics found in plants such as the Space Shuttle Orbiter docked to the International Space Station.

II. Vehicle Dynamics and Phase Plane Control

The rotational equations of motion and kinematics for a spacecraft's principal axes in inertial space, are[1]:

$$
\begin{aligned}
&J_1\dot{\omega}_1 = (J_2 - J_3)\omega_2\omega_3 + T_{1ext} + u_1 \\
&J_2\dot{\omega}_2 = (J_3 - J_1)\omega_1\omega_3 + T_{2ext} + u_2 \\
&J_3\dot{\omega}_3 = (J_1 - J_2)\omega_1\omega_2 + T_{3ext} + u_3 \\
&\eta = \cos\left(\frac{\varphi}{2}\right) \qquad \dot{\eta} = -\frac{1}{2}\varepsilon^T\hat{\omega} \\
&\hat{\varepsilon} = \hat{a}\sin\left(\frac{\varphi}{2}\right) \qquad \dot{\hat{\varepsilon}} = \frac{1}{2}\left(\hat{\varepsilon}^{\times} + \eta I\right)\hat{\omega} \\
&\Lambda_{IB} = \begin{bmatrix}\eta & \hat{\varepsilon}\end{bmatrix}
\end{aligned}
\tag{1}
$$

Where $\hat{\omega}$ and Λ_{IB} are the principal axis angular velocities and attitude quaternion, respectively. The latter is defined by the eigenaxis (or Euler axis) $\hat{a}$ and eigenangle (or Euler angle) φ. The vectors J, T_{ext}, and u are principal moments of inertia, external disturbance torque, and external control torque, respectively.

With an axis of symmetry (J_2=J_3) and ignoring external disturbance and control torques, the dynamics simplify to "torque-free" equations:

$$
\begin{aligned}
&J_1\dot{\omega}_1 = 0 \\
&J_3\dot{\omega}_2 = (J_3 - J_1)\omega_1\omega_3 \\
&J_3\dot{\omega}_3 = (J_1 - J_3)\omega_1\omega_2
\end{aligned}
\tag{2}
$$

A closed-from solution for the body rate time histories can be derived in the absence of external torque (i.e. "torque-free" or "coasting"):

$$
\begin{aligned}
&\omega_1 = \omega_{1_0} \\
&\omega_2 = \omega_{2_0}\cos(\Omega t) + \omega_{3_0}\sin(\Omega t) \\
&\omega_3 = \omega_{3_0}\cos(\Omega t) - \omega_{3_0}\sin(\Omega t) \\
&k = \left(1 - J_1 \big/ J_3\right) \qquad \Omega = k\omega_{1_0}
\end{aligned}
\tag{3}
$$

Where the "0" denotes the initial conditions. It is noted that the frequency content of the coast motion is determined by the inertia ratio and the initial roll rate.

Control for on-off constant force thruster systems generally involves a "deadzone" to avoid high frequency thruster chattering, and the deadzone is commonly implemented in the form of a phase plane control system[2]. Given an error quaternion Λ_e and a rotational rate error vector, the phase plane plots attitude error (ϕ_e) per axis against attitude rate error (ω_e) per axis, and creates a 'deadzone' around the commanded attitude state where no control action is taken. The allowable attitude error is typically called the 'deadband', and the allowable rate error is typically called the 'Rate Limit' (RL). These parameters are shown in Figure 1, where a phase plane is, in its simplest form, defined by linear switching lines. These switching lines are a linear combination of the attitude and rate errors, and when the attitude state is outside of these switching lines, the thrusters are commanded on.

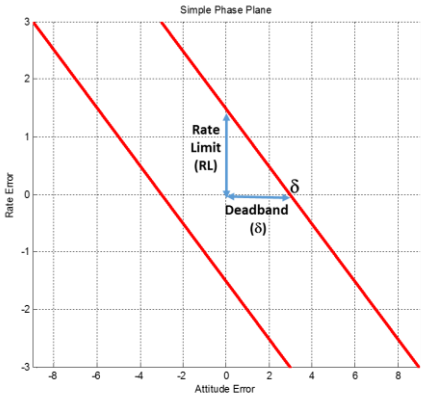

Figure 1. Simple Phase Plane with Deadzone Nomenclature

Typically added to a phase plane design are hysteresis switching lines, where these additional switching lines are added to minimize thruster on-off chattering. This simple control law, specifically using linear switching lines with hysteresis, is commonly called a Schmitt Trigger[2], shown in Figures 2 and 3.

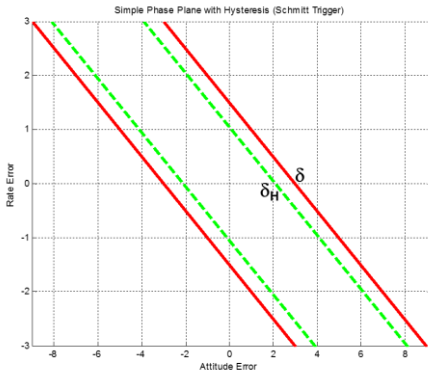

Figure 2. Simple Phase Plane with Hysteresis (Schmitt Trigger)

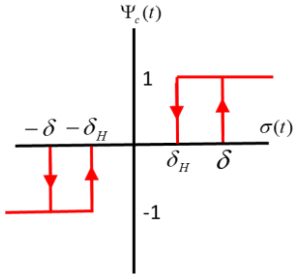

Figure 3. Phase Plane with Hysteresis input vs output (Schmitt Trigger)

Bryson (Reference 2) provided the resulting limit cycle amplitude and period for a phase plane with hysteresis in the absence of external disturbance torques (equation 4).

$$\text{Period} = \frac{4\delta}{RL}\left(\frac{\delta+\delta_H}{\delta-\delta_H}+\frac{\delta-\delta_H}{2a_c\dfrac{\delta}{RL}}\right)$$

$$\text{Amplitude} = \frac{1}{2}\left(\delta+\delta_H\right)+\frac{\left(\delta-\delta_H\right)^2}{8a_c\left(\dfrac{\delta}{RL}\right)^2} \qquad \textbf{(4)}$$

Typically "drift channels" are added to the design to minimize peak rates during control, hence reducing propellant usage. These drift channels reflect a compromise between a minimum time solution and propellant savings when dealing with high rotational rates. A phase plane design using both drift channels and hysteresis is shown in Figure 4. This design was employed for the Reaction Control System for the Ares 1/I-X launch vehicles. In this design, the hysteresis for the drift channel is defined at its center.

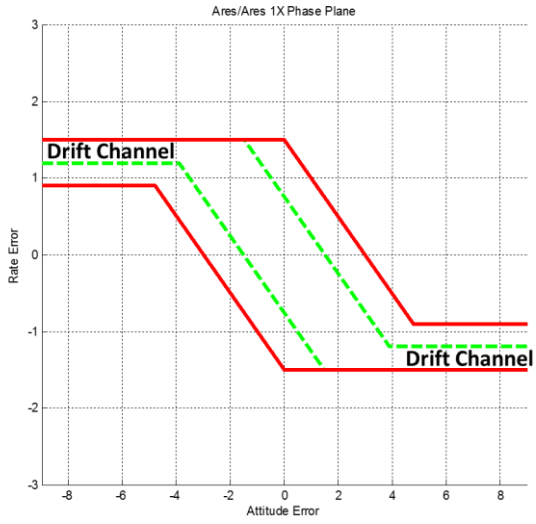

Figure 4. Ares I/Ares I-X Phase Plane

A phase plane trade study was performed for the different coast stages of the EUS vehicle trajectory using a 3-DOF (rotation-only) time domain simulation (Figure 5) using the Ares I phase plane design (Figure 4). The addition of hysteresis resulted in a significant reduction in thruster duty (on-off) cycles. Fuel savings can be realized as well, however hysteresis generally changes the firing pattern when a system accommodates a disturbance, not total integrated impulse.

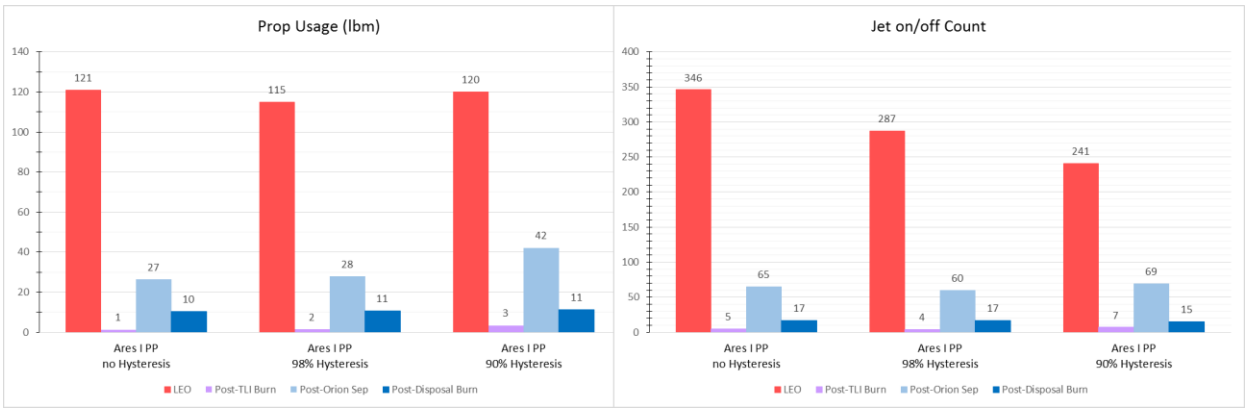

Figure 5. Vehicle Control Performance With and Without Hysteresis

Using Disturbance Estimate in Phase Plane Switching Line Definition

For configurations where vehicle external disturbances are large relative to control authority, and/or where thruster duty cycles are a concern, it may be beneficial to estimate vehicle disturbance acceleration and use this estimate in the definition of the phase plane switching line[3]. This logic was employed in the Apollo[4] and Space Shuttle orbiter[6] phase plane designs, where the switching lines are parabolic reflecting the effective control authority given external disturbance. The hysteresis line for these designs, shown in green in Figure 6, works to establish a phase plane limit cycles with a magnitude of ½ of the commanded deadband. One risk of using disturbance estimation in the phase plane definition is that poor disturbance estimation can lead to poor phase plane limit cycle performance, where, for example on Space Shuttle Flight STS-71, the first flight where the shuttle docked to the Russian MIR, unmodeled Shuttle RCS self-impingement on the Shuttle structure led to an inaccurate estimation of a high external vehicle disturbance, significantly increasing propellant consumption[5].

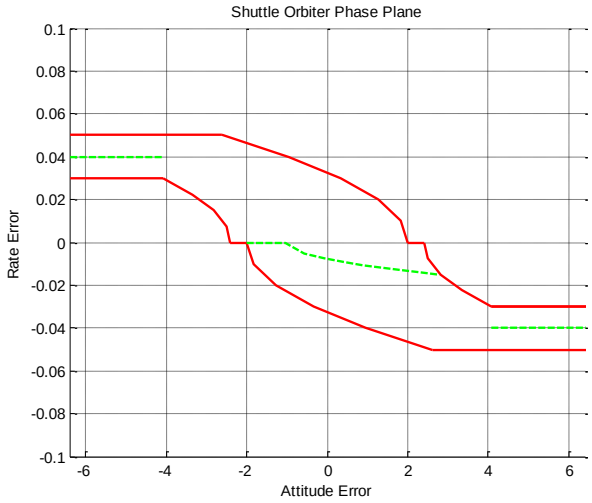

Figure 6. Space Shuttle Orbiter Phase Plane

Partial Commands for State Errors inside Deadzone

The Space Shuttle phase plane design would allow the phase plane algorithm to issue partial commands (a command with magnitude greater than zero but less than one) provided at least one other axis is outside the deadzone[6]. This partial command logic allows the resulting thruster acceleration to correct smaller errors, even while inside the deadzone, while correcting error in a different axis. For example, if the rate error has a magnitude of half the rate limit, then the partial command could be 0.5. This increase in complexity is likely more useful with configurations where uncoupled single axis accelerations are not generally available (say with diverse mass properties or non-orthogonal thruster configurations).

The phase plane designs shown in Section II represent a basic architecture for a control law employing on-off thrusters. More complex pulse width modulation approaches are available as well, for example see Reference 7. The phase plane control law, however, is nonlinear, hence stability analyses of the system must employ nonlinear control system analysis approaches (see section III).

III. Phase Plane Stability and Filter Design

It is necessary for flight vehicle certification to demonstrate stability of the system/vehicle dynamics and disturbances such as environmental torques, flex/slosh dynamics, and system latencies. Typical stability margin definitions are shown in Figure 7, with typical design standards[8] shown in Table 1. Note with nonlinear phase plane control, these linear-based margin definitions are not directly applicable.

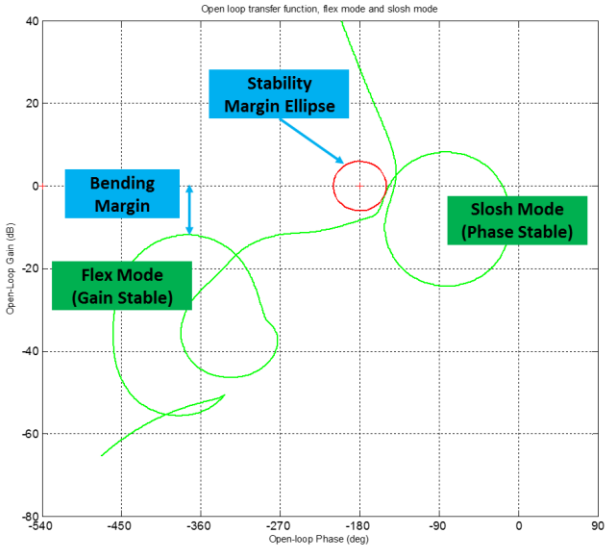

Figure 7. Typical Stability Margin Definitions

	Margin Type	Rigid Body	Slosh (Phase Stabilized)	Slosh (Gain Stabilized)	Bending (Gain Stabilized)
Nominal	Ellipse	Ellipse with axes of +/- 30 deg in phase and +/- 6 dB in gain			
	Peak Amplitude	N/A	< +10 dB	N/A	< -10 dB
Dispersed	Ellipse	Ellipse with axes of +/- 20 deg in phase and +/- 3 dB in gain			
	Peak Amplitude	N/A	N/A	N/A	< -6 dB

Table 1. Space Launch System (SLS) Ascent Stability Margin Design Criteria[8]

Given the nonlinearity of the phase plane, or any other related formulation employing a deadzone, analysis and stability margin computations will fall within the category of either performing nonlinear analysis of the nonlinear system, or developing a linear approximation of the nonlinear components. The former, using nonlinear analysis approaches, generally involves formulating the problem with the nonlinear components separated from the linear portion of the plant (as with the Lure formulation), then using sufficient conditions like those associated with the Circle Criterion[9] or Describing Functions[10]. In the latter, performing a nonlinear analysis using Describing Functions (DF), it involves the prediction of any flex-induced limit cycle by comparing the nonlinear Describing Function with the Linear Plant. In this case, the existence of a sustained flex-induced limit cycle is considered unstable performance[10]. Alternatively, one can develop a linear approximation of the nonlinear phase plane component, which allows traditional control theory linear analysis. Two approaches of linearization are using Pulse Width Modulation (PWM) such as used in the International Space Station (ISS) design[11], or describing functions. In this paper we concentrate on the latter approach. Good correlation between the stability results of these various analysis approaches has been demonstrated[12].

A simplified phase plane control system model[9] is shown in Figure 8, shown here as a single axis regulator problem (commanded attitude and rates =0). For a given input command (Ψ), the jet select represents the algorithm used to choose which thrusters to fire to accommodate the rotational command, supplying vehicle acceleration. Jet Selection may be table-lookup or a more complex scheme as discussed in section IV. The plant contains rigid, flex, and slosh dynamics in response to the thruster acceleration input. Sensor dynamics contain the frequency response of the sensor hardware, including internal anti-aliasing filtering. The flex filter block consists of a set of filtering, low pass in nature, to attenuate high-frequency dynamics and noise while at the same time allowing low-frequency dynamics to feedback into the controller. System latency includes system transport lags as well as latencies associated with digital algorithm execution. The phase plane control system generates a rotational command using attitude error and rate error input, employing a deadzone to minimize propellant usage. The phase plane design may include hysteresis, drift channels, etc., to further regulate propellant usage and thruster duty cycles. The phase plane controller is a nonlinear component, which leads to the need for nonlinear analysis approaches for stability determination. The phase plane autopilot produces a single command per axis that takes, in its simplest form, one of three options; 0 for no-firings (the error state is inside the deadzone) +1 for positive rotational acceleration command and –1 for negative rotational acceleration command. This command is sent to a jet selection logic that determines the thrusters to best achieve the command, completing the loop. The phase plane design is generally dictated by performance considerations (for example "tight" control may be needed to support vehicle separation operations), while the key design challenge is the development of the flex filtering (software) to ensure stability, both rigid body and in the presence of disturbances such a vehicle flexure.

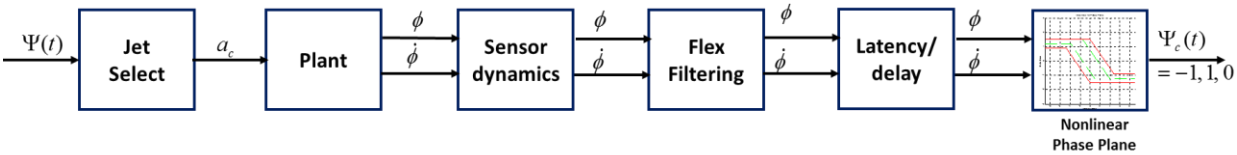

Figure 8. Phase Plane Control System Model with Phase Plane Nonlinearity

As mentioned previously, two approaches to analyze system stability with the nonlinear phase plane component are to either separate the nonlinear from the system using nonlinear analysis approaches such as describing functions or Circle/Popov Criterion, or to develop a linear approximation of the nonlinear system by using linearization approaches such as PWM or describing functions. This paper will examine the latter (developing a linear approximation of the nonlinear system) using describing functions.

To use describing functions to develop a linear representation of this nonlinear phase plane controller, first transform the phase plane controller into an equivalent Proportional Derivative (PD) system followed by an ideal relay, as supplied by Jang, et.al, in Reference 9. For simplicity in this discussion we will remove the sensor dynamics (generally having high frequency bandwidth) and the jet select from Figure 8, resulting in:

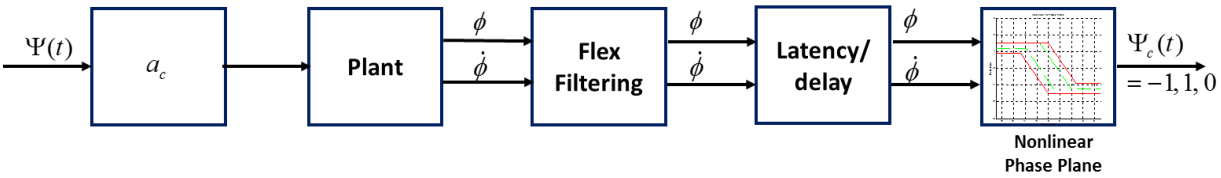

Figure 9. Simplified Phase Plane Control System Model with Phase Plane Nonlinearity

The PD control law is based on the inverse slope of the switching line (***τ=δ/RL)***, consistent with Schmitt Trigger definition[2]. This representation allows the deadzone to be modeled as an ideal relay[9]:

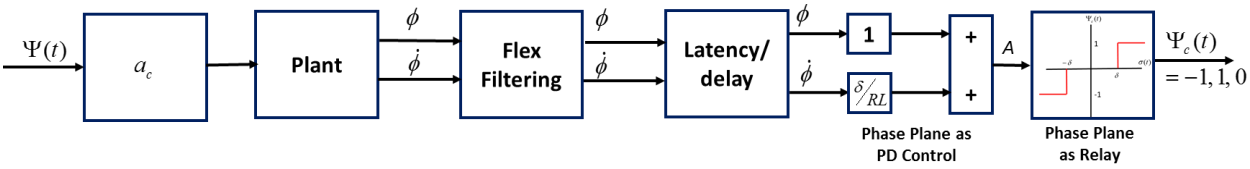

Figure 10. Simplified Phase Plane Control System with Phase Plane Modeled as PD/Relay Combination

The ideal relay in Figure 10 can be replaced with a describing function to linearize the system[13] and allow frequency response analysis. The describing function for an ideal relay is:

$$N(A) = 0 \qquad A < \delta$$
$$N(A) = \frac{4}{\pi A}\sqrt{1-\left(\frac{\delta}{A}\right)^2} \qquad A > \delta \tag{5}$$

In this application, the describing function is a nonlinear loop-gain representation of the phase plane. At this point this representation is still a nonlinear function since the loop gain is dependent on the input magnitude (A). Physically, the amplitude A represents the magnitude of the attitude state error with respect to the deadband (δ). When A is less than δ, there is no control, and hence the loop gain is zero. When A is greater than δ, the thrusters will fire, and the equivalent linear loop gain is a function of the input error A magnitude. To complete the linearization of this system, a value of A must be chosen, and we choose the value (A^*) to maximize the value of the loop gain (i.e. maximizing the describing function maximizes the loop gain). Maximizing the loop gain represents the peak response of the thrusters to state error, and maximizes the gain on the flex dynamics amplitude (hence conservative). The peak value of a describing function for an ideal relay occurs when:

$$A^* = \sqrt{2}\delta \qquad \rightarrow \qquad \mathrm{N}\left(\mathrm{A}^*\right) = \frac{2}{\pi\delta}$$

Hence the linear representation of the phase plane system becomes:

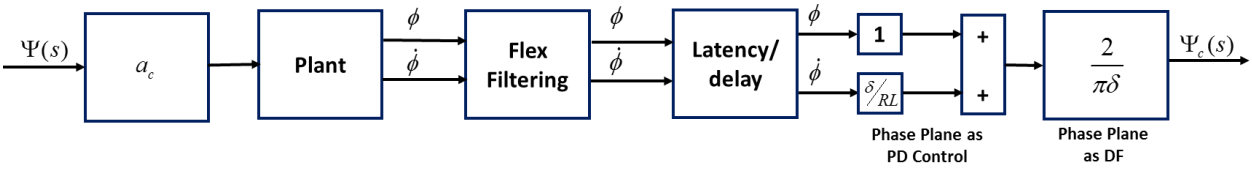

Figure 11. Simplified Phase Plane Control System with Phase Plane Modeled as PD/Relay Combination

One advantage of using a describing function for phase plane representation is that hysteresis can be modeled by using the appropriate describing function. For example, the describing function representing the hysteresis shown in Figure 2 is below[13]. To utilize this describing function in a block diagram to represent a phase plane, again find the value of *A* which maximizes *N(A)*.

$$N(A) = 0 \qquad \mathrm{A} < \delta$$

$$N(A) = \frac{2}{\pi A}\left[\sqrt{1-\left(\frac{\Delta}{\mathrm{A}}\right)^2(1-\lambda)^2} + \sqrt{1-\left(\frac{\Delta}{\mathrm{A}}\right)^2(1+\lambda)^2}\right] - j\,\frac{4\Delta}{\pi A^2} \qquad \mathrm{A} > \delta$$

$$\Delta = \frac{\delta - \delta_H}{2} \qquad \lambda = \frac{\delta + \delta_H}{2\Delta}$$

Phase Plane Rigid Body Stability Analysis

To show application of the phase plane model linearized with the use of a describing function, we take the example of rigid body control, bending filters removed, and ideal latency (T_D) in both the attitude and rate channels. This simplified system is shown in Figure 12 where it is noted the equivalent proportional and rate gains for the phase plane are inversely proportional to the attitude deadband and rate limit, respectively:

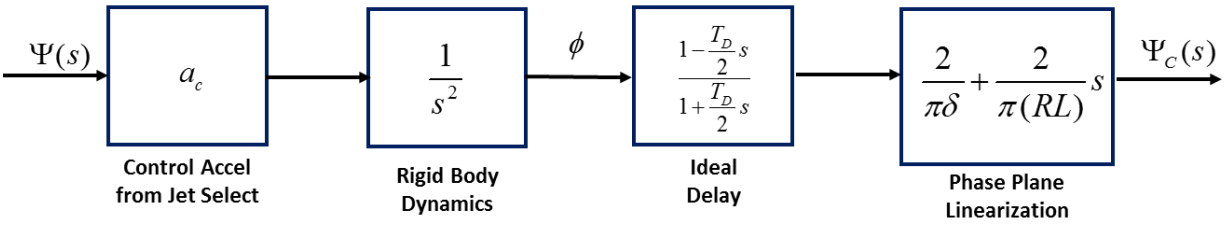

Figure 12. Simplified Rigid Body System with Phase Plane Modeled as PD/Relay Combination

The closed loop transfer function for this system with unity feedback is:

$$\frac{\Psi_c(s)}{\Psi_c(s)} = \frac{\frac{2a_c}{\pi}\left[-\frac{T_D}{2(RL)}s^2 + \left(\frac{1}{RL} - \frac{T_D}{2\delta}\right)s - \frac{1}{\delta}\right]}{\frac{T_D}{2}s^3 + \left(1 - \frac{a_c T_D}{\pi(RL)}\right)s^2 + \frac{2a_c}{\pi}\left(\frac{1}{RL} - \frac{T_D}{2\delta}\right)s + \frac{2a_c}{\pi\delta}}$$

The following stability condition (equation 6) is derived from Routh's Stability Criterion.

$$\frac{1}{RL} - \frac{T_D}{\delta} - \frac{a_c T_D}{\pi(RL)^2} + \frac{a_c T_D^2}{2\pi(RL)\delta} > 0 \tag{6}$$

Hence, for stability, given a vehicle's control acceleration (a_c), latency (T_D), and desired attitude rate limit (RL), the deadband must be greater than the value shown in equation 7.

$$\delta > \frac{T_D - \frac{a_c T_D^2}{2\pi(RL)}}{\frac{1}{RL} - \frac{a_c T_D}{\pi(RL)^2}} \tag{7}$$

Or likewise, for stability, given a vehicle's control acceleration (a_c), desired deadband (δ), and desired attitude rate limit (RL), the latency must be less than the value shown in equation 8.

$$T_D < \frac{a_c\delta - \left(a_c{}^2\delta^2 + \pi^2(RL)^4\right)^{1/2} + \pi(RL)^2}{a_c(RL)} \tag{8}$$

Example: Pitch Phase Plane Control with NASA EUS Vehicle

The above stability condition derived from a phase plane linearization using a describing function shows an allowable latency of 3.7 seconds for the EUS mass properties and typical phase plane design (δ=0.6 deg, RL = .15 deg/sec). Nonlinear simulation modeling an actual phase plane control law, with nonlinear plant dynamics, shows consistency with this result, with RCS stability with a delay of 2.5 seconds (Figure 13), and unstable control with a delay of 4 seconds (Figure 14).

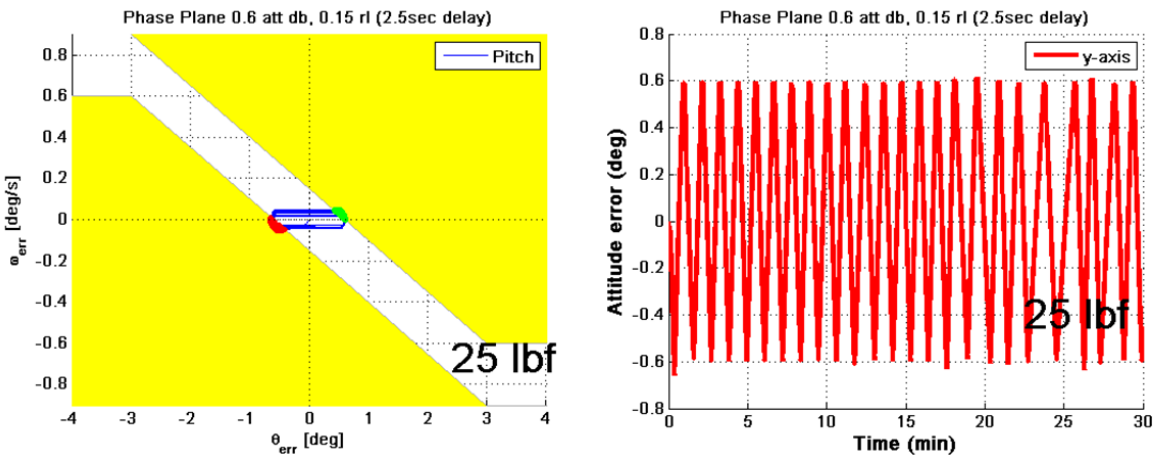

Figure 13: Nonlinear Time domain Simulation Showing Stable Control with a Latency of 2.5 seconds. Linearized model using Describing Function Approach predicted instability at Latency of 3.7 seconds.

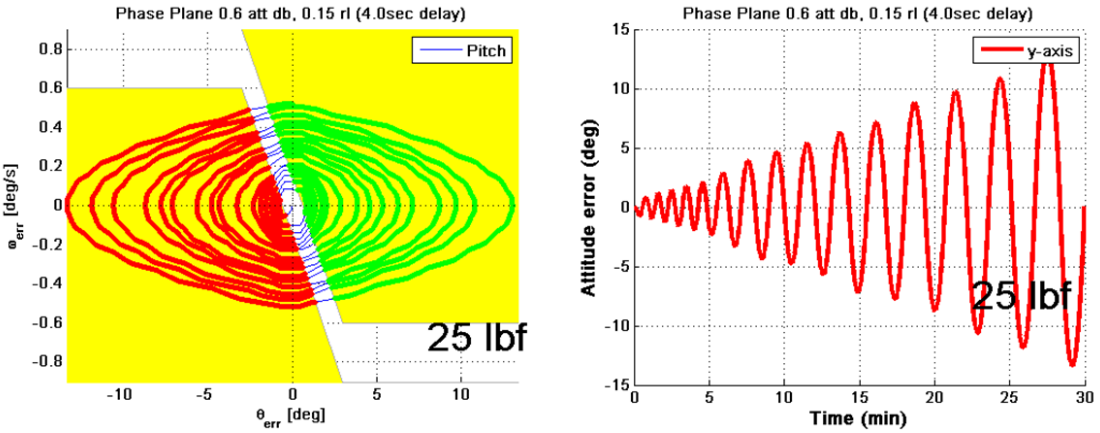

Figure 14: Nonlinear Time domain Simulation Showing Unstable Control with a Latency of 4 seconds. Linearized model using Describing Function Approach predicted instability at Latency of 3.7 seconds.

Filter Design to Ensure Stability of a Phase Plane Control System

A key design challenge in developing the on-orbit flight control software is the development of the software filtering to ensure control system stability. Four design considerations for developing these filters are summarized below.

Key Filter Design 1: Rigid body Stability

A principal concern with space vehicle rigid body stability is adequate margin to accommodate system latencies, which is measured in the form of available phase margin. The above analytical solution for allowable latency (equation 8) is derived to compute allowable latency for the simple system in Figure 12, however analytical solutions are not so available when higher order dynamics are added to the plant or high-order filters are added to attenuate noise and vehicle flex dynamics. Margin to system latencies can be determined graphically by observing the frequency of the rigid body cross-over point in the Nichols Plot (Figure 15). In this example, allowable latency is easily computed from the relationship between the rigid body cross-over frequency (ω_{CR}) and rigid body phase margin (θ_R):

$$T_D(\text{sec}) < \frac{\theta_R(\text{deg}) - 180}{(360\,\text{deg})\omega_{CR}(Hz)} = \frac{195 - 180}{360 * 0.0167} = 2.5\,\text{seconds}$$

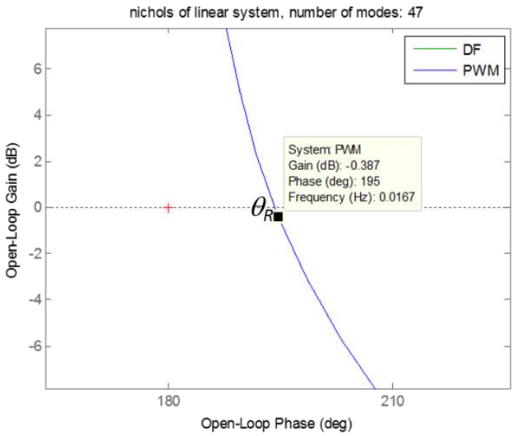

Figure 15. Graphic Determination of Allowable Latency (T_D) Given Rigid Body Phase Margin (θ_R) and Rigid Body Cross-Over Frequency (ω_{CR})

Another key aspect for rigid body stability is to ensure the capability to estimate the frequency content associated with the gyroscopic torques in the nonlinear rigid body dynamics (equation 1). This is accomplished by ensuring the system phase lag associated with gyroscopic torques, which is defined by omega (Ω) in Equation 3 for a vehicle with inertial symmetry, is small, with a peak acceptable lag being 90 degrees[14]. Note this frequency, for a vehicle with inertial symmetry, is proportional to the rotational rate about that axis of symmetry, and hence a relationship exists between filter phase lag and maximum allowable rotation rate.

Key Filter Design Principal 2: Flex Gain Margins

Flex corruption in the measured sensor content can drive an RCS system unstable. Typically this instability manifests itself in the form of steady-state rate-limit limit cycles, as shown in Figure 16. Less common, attitude limit cycle instabilities may occur as well, and can be experienced with operations requiring tight attitude control[15]. RCS stability is generally achieved by filtering of the rate sensor data, and likely the attitude data is well. Shaping of the commanded thruster firing frequency content, say through command shaping (Section IV), is an alternative approach to minimize flex amplitude (and gain confidence in stability) but generally less common due to concern with robustness.

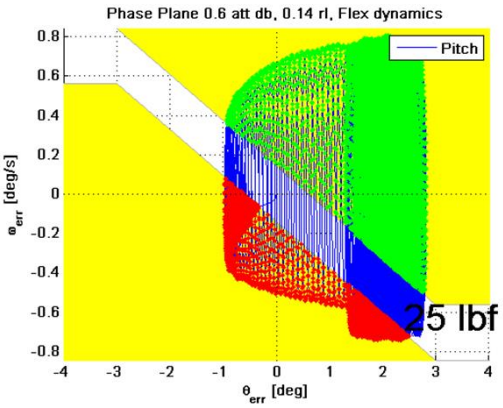

Figure 16. Phase Plane Flex Induced Instability. Colors Denote Firing Command Directions: Green = -1, Blue = 0 (Off), Red = +1

RCS stability given a flex environment can be demonstrated using the linearized approaches described above, specifically using DF or PWM approaches to linearize the nonlinear phase plane in the system definition. This provides a sufficient condition for stability, and an initial design metric for the corresponding filter design. Flex modal frequencies are typically much higher in frequency than the rigid body frequencies of concern, hence the flex modes are targeted to be gain-stabilized, where the corresponding filters are designed to provide adequate attenuation to ensure stability. An example of flex-body stability margins is shown in Figure 17, where the flex mode attenuation meets the requirements from Table 1. In this figure, good correlation is noted when frequency response is computed via Pulse Width Modulation (PWM) vs. Describing Functions (DF).

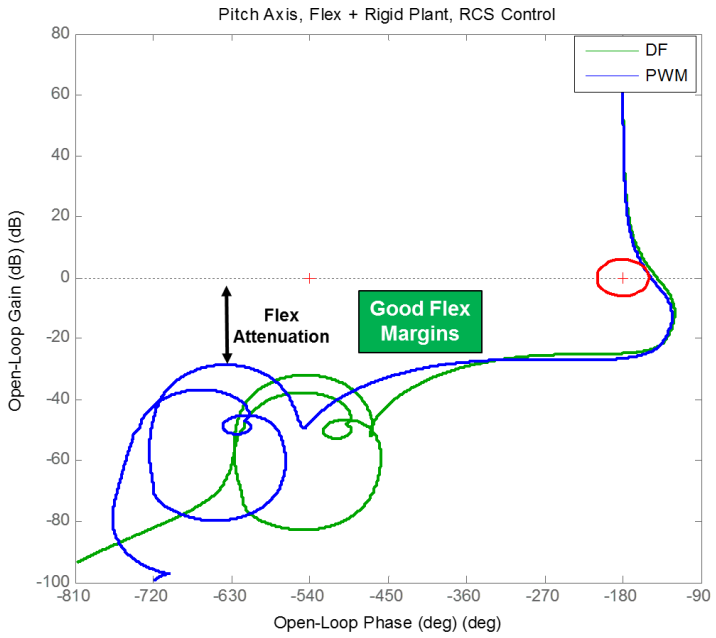

Figure 17. Flex Body Stability Results: Adequate Flex Margins Demonstrated by both DF and PWM Approaches

When the vehicle flex modes are lower in frequency, using the stability (sufficient) condition from DF or PWM may be too conservative to allow as a metric for filter design. This was typically the case for Space Shuttle on-orbit operations, such as where the Shuttle controlled the docked ISS configurations. Hence a less-conservative forcing function approach was utilized by Shuttle for these configurations, explained below.

It is considered necessary and sufficient for RCS flex mode gain stability if the peak flex excitation caused by a worst-case firing pattern does not exceed the rate limit value. For Shuttle application, this worse case firing pattern is defined as four bi-polar pulses occurring at the half-period of the flex mode of concern[5]. These four pulses physically represent the RCS correcting a rate error, then commanding a maneuver rate, then damping the maneuver rate, then performing a final rate correction. This forcing function criteria proves much less conservative than the previously mentioned DF or PWM approach, as shown in Figure 18 for a low frequency flex mode. In this example, the low frequency flex excitation fails the sufficient condition provided by the DF, but shows adequate stability margin when using the less-conservative forcing function approach. This four-pulse bi-polar forcing function was used in Shuttle/Station loads analysis as well to define peak structural loads due to RCS firings.

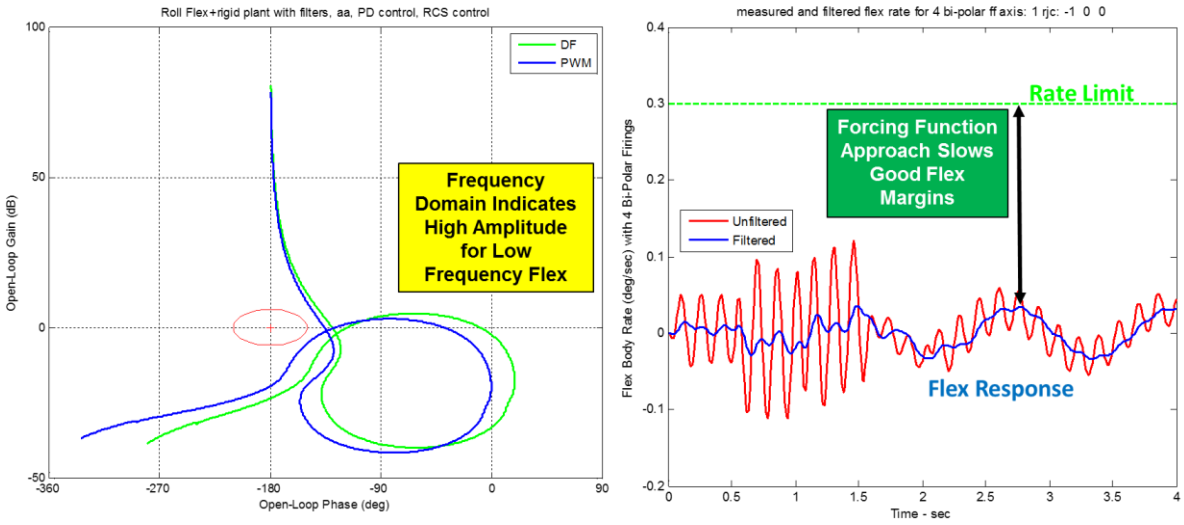

Figure 18. Stability Analysis shows Solar Array Flex Non-Compliance with DF-derived Sufficient Condition, but Adequate Margins Using less-Conservative Forcing Function Approach

The above approach for flex mode gain stabilization with RCS is generally available when the modal frequencies are separated in frequency (higher) from the rigid body modes to allow gain stabilization. If not, then phase stabilization[14] may be necessary, where the control designer must ensure that the system phase lag is sufficiently small at the modal frequencies to allow active suppression of any flex excitation.

Key Filter Design Principal 3: Minimizing Filter Induced Lag

Lag introduced by the bending filters can lead to poor knowledge of the actual rate during a thruster firing, resulting in phase plane overshoot and increased propellant consumption. This is illustrated in Figure 19, where filter induced lag results in completely overshooting the phase plane rate limit. To analyze this and develop a design criteria, the rate change during a thruster firing is modeled as a ramp[16], and the filter lag response to the ramp input is determined.

One can analytically estimate the peak allowable filter lag (T_F), in seconds, which "breaks" the phase plane design:

$$T_F = \frac{RL}{a_c} - \text{other system lags} \qquad \textbf{(9)}$$

This maps into a filter phase constraint as a function of frequency and provides a phase response requirement as shown in Figure 20:

$$\text{allowable filter phase lag (deg)} = T_F\,(\text{sec}) * (\text{freq in Hz}) * 360 \qquad \textbf{(10)}$$

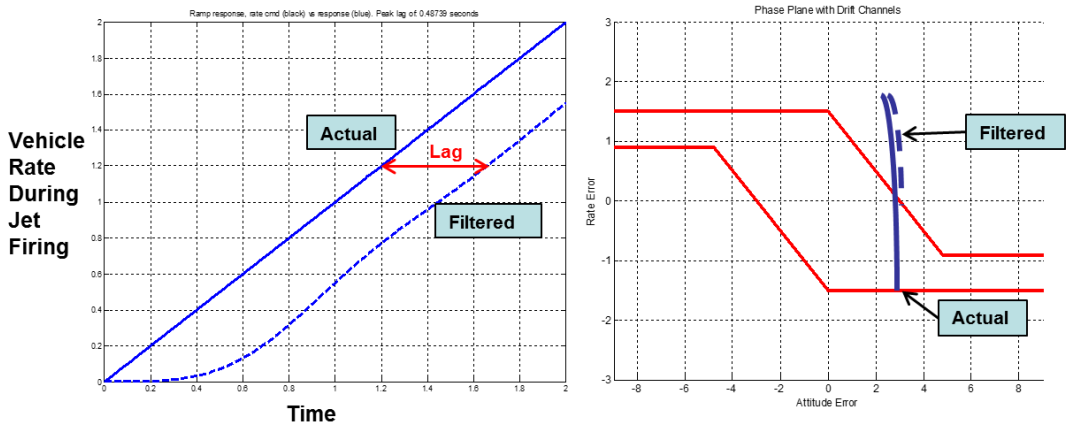

Figure 19. Filter Induced Lag Results in Phase Plane Overshoot

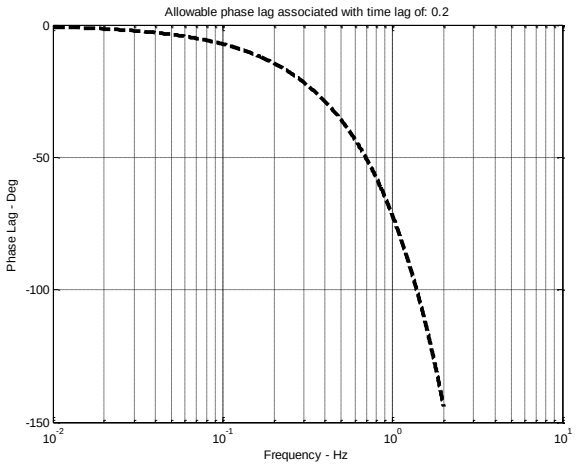

Figure 20. Filter Phase Design Constraint for allowable filter lag of 0.2 seconds.

Time Domain Simulation filter lag constraint from equation 10 shows good correlation with propellant usage in high fidelity nonlinear simulation (Figure 21), where the latency magnitude defined by equation 9 does indeed "break" the phase plane design and, at that point, results in significant propellant use increase.

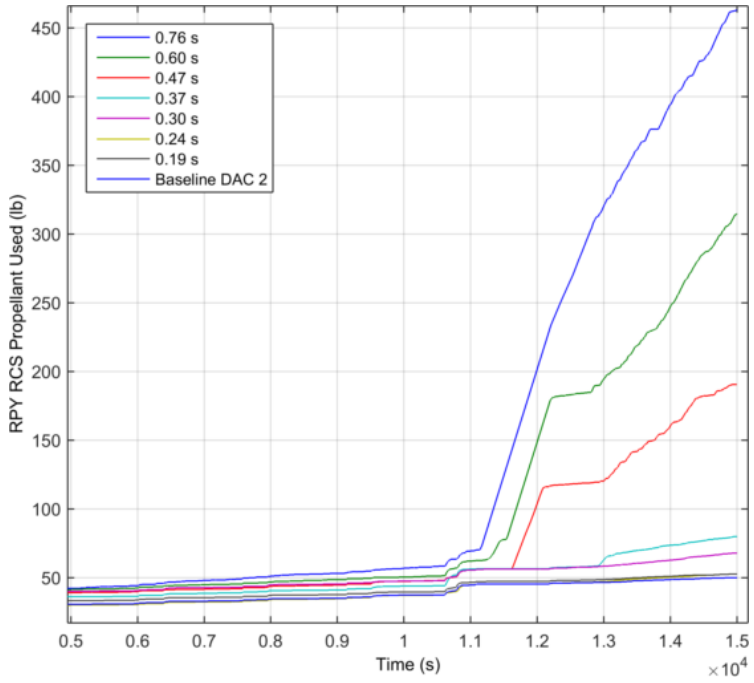

Figure 21. Propellant Usage for Differing Filter Phase Lag

Key Filter Design Principal 4: Feed Forward during Thruster Firings

As stated earlier, a key consideration when designing software filters for RCS control system stability is minimizing the filter-induced lag during thruster firings, as this lag can result in phase plane overshoot and significant propellant usage increase. An alternative approach to minimize this sensitivity, and allow a significant decrease in filtering bandwidth, is to feed-forward estimates of thruster acceleration during thruster firings. For the Space Shuttle, this allowed significantly lower bending filter bandwidth that was necessary to stabilize the control system with the very low frequencies associated with the docked ISS operations. Figure 22 shows a conceptual diagram of the Shuttle rate filter[16], where thruster acceleration feed-forward was computed from the Initialization Load (I-Load) mass property values and then physically added to the rate during thruster firings. In this case, the filter converges on the error in the feed-forward estimate rather than the overall vehicle rotational rate.

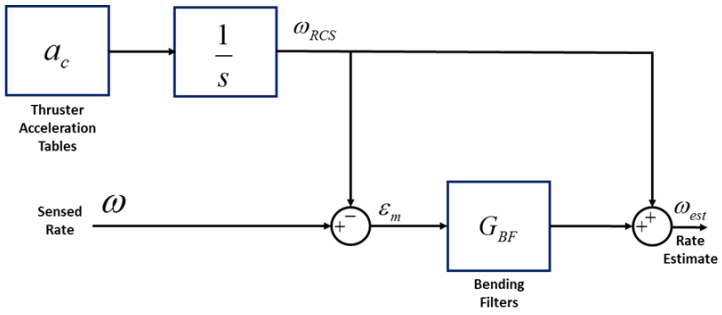

Figure 22. Shuttle Conceptual Implementation of Rate Estimation Using Feed-Forward

RCS Off-axis Control During Powered Flight

A typical role for RCS control is to provide roll control during single-engine powered flight, where the single-engine Thrust Vector Control (TVC) gimbal system can provide for control in the pitch and yaw axes, but not roll. For example, the Ares I-X vehicle used a single engine during ascent, hence roll control during ascent was provided by a separate RCS system using the phase plane in Figure 4. In this operation, the RCS system must be designed to accommodate the roll disturbance torques associated with the pitch/yaw TVC gimbal motion and other disturbance sources, as well as demonstrate RCS stability during the powered flight. We define a sufficient condition for RCS stability during powered flight:

It is sufficient for roll RCS stability during single-engine TVC burns if the peak filtered roll rate for a worst case pitch/yaw TVC excitation is smaller than the roll phase plane rate limit.

This sufficient condition means that, even given the peak roll flex rate excitation at steady state due to the worst-case pitch (or yaw) TVC command, the roll axis phase plane will not respond. The process for generating this model is to define the Laplace Transform from the pitch (or yaw) TVC command to roll flex rate (Figure 23), and multiply it by the peak allowable gimbal command magnitude (Figure 24). This then physically represents the peak steady-state flex roll rate for a pitch (or yaw) gimbal sine-wave resonating the roll structural modes. If feasible from a standpoint of performance, roll bending filters can be designed to achieve this sufficient condition, with margin, hence demonstrating adequate stability.

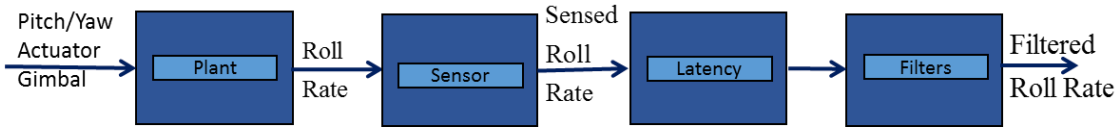

Figure 23. System of Roll Rate Response for Pitch/Yaw TVC Commanding

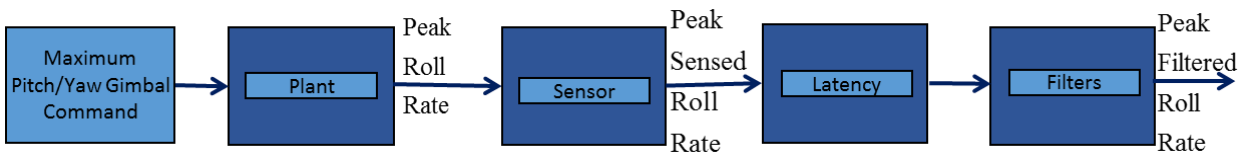

Figure 24. System Producing Peak Steady State Roll Flex Rate Given Worst Case Pitch/Yaw TVC Input

An example of this application is shown in Figure 25, where the peak steady state roll rate resulting from a four degree TVC excitation results in meeting the sufficient condition, i.e. the peak possible roll rate is within the phase plane rate limit. Note that failing to meet this sufficient condition generally means higher fidelity analysis is needed as this sufficient condition is obviously conservative.

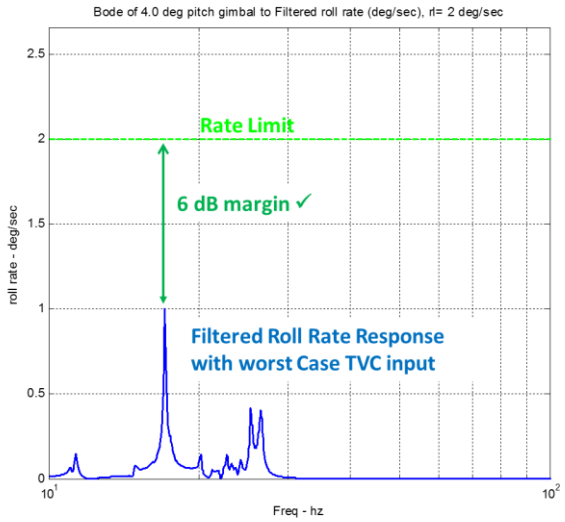

Figure 25. Example Showing Peak Steady State Flex Body Roll Rate within Phase Plane Rate Limit for a Peak Pitch/Yaw Gimbal Excitation

IV. Jet Selection

Jet Selection is the software algorithm used to determine which thrusters to fire given a command. The input command is commonly a rotational command vector, capturing the three degrees of freedom of rotational space (roll/pitch/yaw). For the Space Shuttle Primary Reaction Control System (PRCS) thrusters, this command could be six degrees of freedom, where the thruster selection would be required to accommodate a joint rotational/translational command.

Table Look-Up Jet Select

Generally a thruster selection software algorithm is a table-lookup scheme, which works well when the thruster configuration is orthonormal to the vehicle body axes, and where the range of anticipated vehicle mass properties is well known. The software for a table-lookup jet selection is generally minimal for a configuration using a small number of thrusters, even when including logic for thruster failures. The Space Shuttle PRCS, using 38 thrusters to control six degrees of freedom, employed a complex table look-up algorithm using Boolean logic[6].

For Space Shuttle rotational control, however, where a large range of mass property configurations were realized (ranging from payloads deployed on the Shuttle arm to configurations when docked to the International Space Station), multiple closed-form jet selection algorithms were analyzed beyond Table-lookup. These included a jet selection to maximize angular acceleration given a command ("dot product jet select"), a jet selection to minimize acceleration error given a command ("minimum angle jet select"), a fuel-optimal jet selection, and jet selection employing load-limiting pre-shaping. These are discussed in more detail below.

Space Shuttle Dot Product Jet Select

The Space Shuttle Dot product jet selection algorithm chose up to three thrusters given as input the desired rotational velocity increment (or acceleration) by taking the dot product of this three axis command with the rotational velocity increment (or acceleration) vector of each thruster. The thruster with the largest dot product magnitude is fired, and a second thruster is fired if its dot product magnitude is 50% of the first, and a third thruster is fired if its

dot product magnitude is 40% of the first. The magnitude thresholds for the second and third thruster (50% and 40%) were variable by software gains (I-Loads), however rarely if ever changed. See Figure 26.

Space Shuttle Minimum Angle Jet Select

The Space Shuttle Minimum angle jet selection algorithm[18] chooses up to three thrusters given as input a desired rotational velocity increment (or acceleration) by minimizing the angle between this three axis command and the resulting rotational velocity increment (or acceleration). To minimize this angle, effectively minimizing undesired cross-coupling, even thrusters that reduced overall resulting acceleration would be considered as a firing candidate, given a command, if it removed undesired off-axis acceleration. Minimal acceleration checks were included to ensure propellant efficiency[17]. See Figure 26. For configurations where the Shuttle was docked to the ISS, a very challenging control problem, the minimum angle jet select nearly always out-performed the dot product jet select. For those configurations, minimizing thruster cross-coupling and undesired off-axis accelerations (Minimum Angle Jet Select) proved more beneficial than maximizing resulting acceleration (Dot Product Jet Select).

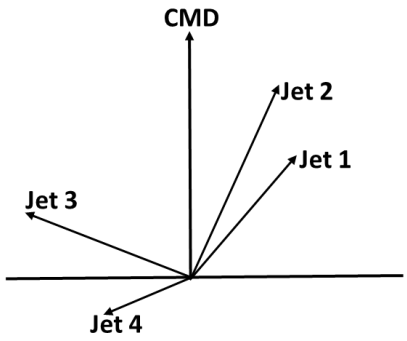

Figure 26. Two Space Shuttle Jet Select Options for a Given Command (CMD): Dot Product Jet Select would choose Jet 1 and Jet 2, while Minimum Angle Jet Select would choose Jet 2 and Jet 4.

Optimal Jet Select

Jet selection algorithms to achieve a fuel-optimal firing pattern for a given rate command are available. The problem formulation[32] follows such that given a *b* vector whose elements are the desired rate changes for *m* degrees of freedom and a matrix A_{jets} whose columns are the accelerations of *n* jets, then the problem is to find the solution for thruster on-times (*x*)

$$A_{jets}x = b \quad x \geq 0$$

such that the cost function *P*, corresponding to propellant usage, is minimized. In this equation, *c* is the n-vector whose elements are the flow rates for the n individual thrusters.

$$P = c^T x$$

Solutions to this problem can be found either with linear programming[18] or analytically[19]. See Reference 7 for a detailed summary of the latter derivation. One challenge to implementing an optimal jet selection algorithm with a phase plane controller is that a fundamental phase plane algorithm provides directional commands, not commanded rate change. An adaption of a phase plane controller to accommodate an optimal jet select rate command was provided by Kubiak[20], however an alternative approach is to integrate the rate error to define attitude error. Optimal jet selection logic was not implemented in the actual Space Shuttle flight control system logic except for testing of advanced control algorithms[18].

Command PreShaping

In many cases thruster firing patterns need to be constrained to minimize structural loading. Often referred to as 'command preshaping', this is not a jet selection per say, but rather an approach to shape the thruster firing durations, and delays between firings, i.e, control the firing frequency content and minimize structural excitation. These approaches were used extensively for Space Shuttle RCS control during payload operations, notably when docked to the International Space Station. Options for command preshaping include targeting specific modes for suppression[21], or a general solution minimizing power spectral density over a band of frequencies[22].

V. Maneuver/Steering Algorithms

Two primary categories of spacecraft rotational maneuver algorithms are minimal time solutions and minimal fuel solutions. For commercial applications the designs generally concentrate on the latter, maneuver trajectories with propellant conservation as a key consideration, and this approach is addressed here. Generally, an rotational error quaternion (Λ_e) and a peak rotational rate magnitude (ω_m) are key inputs into a rotational maneuver algorithm.

Eigen Axis Rotations

The fundamental algorithm for a spacecraft maneuver is based on Euler's Theorem, which states the general motion of a rigid body with one fixed point (specifically the center of mass), is a rotation about an axis through the point. The axis is the Eigenaxis $\hat{a}_e$, derived from the error quaternion Λ_e. This type of algorithm is fundamentally a two pulse bang-off-bang algorithm, where ideally only two firings are utilized, one to begin the rotation and one to end it. An eigenaxis trajectory does not consider the environmental disturbances during the rotation, hence this simplification will result in a propellant penalty. Generally, many more thruster firings will occur during the intended "coast" between firings due to uncompensated disturbances tending to drive the vehicle from the intended coast state. Typically, the peak allowable maneuver rate is specified, ω_m, and hence the commanded rotational rate for the maneuver is simply the desired maneuver rate projected onto the eigen (or Euler) axis $\hat{a}_e$ (Reference 23). The eigenaxis is recomputed each control cycle, and closed-loop control maintained during the maneuver.

Likewise the attitude error per axis can be determined by projecting the eigenangle (ϕ_e) onto the eigenaxis $\hat{a}_e$. Variations off these basic eigenaxis calculations are typical to save propellant or increase performance, such as computing the desired attitude by propagating the commanded rate, or using knowledge of available control acceleration to better reflect anticipated rate error when building to peak commanded rate (ω_m), using knowledge of initial conditions and vehicle acceleration when computing the commanded axis[24], including orbital rate when maneuvering with respect to a local (earth fixed) frame, etc.

Torque-Free Rotations

It was recognized early in spacecraft control research [25, 26] that propellant savings can be realized if the maneuver algorithm follows the natural "torque-free" trajectory. With this approach, unlike an eigenaxis rotation, the vehicle will (ideally) naturally coast to the desired attitude rather than fighting the environmental disturbances. Since a wide range of spacecraft vehicle has an axis of inertial symmetry, the equations of motion for the torque-free trajectory simplify (equation 2). Despite the simple appearance of these equations, no analytical solution exists to derive initial body rate commands (ω_0 from equation 3) to coast "torque-free" to the desired attitude. The Russian MIR vehicle did however employ an approximate solution to these equations using a least squares solution[27]. A closed-form approximate solution to this torque-free problem has been derived which has been used to compare performance of this algorithm against the previously mentioned eigenaxis algorithm (Figure 27). Generally, the torque-free trajectory should provide propellant savings over an eigenaxis rotation, however this depends on the initial conditions of the specific rotation and vehicle-specific control authority distribution between axes. Cost functions can be used to determine which of the two, eigenaxis or torque-free, is the more propellant-efficient trajectory[28].

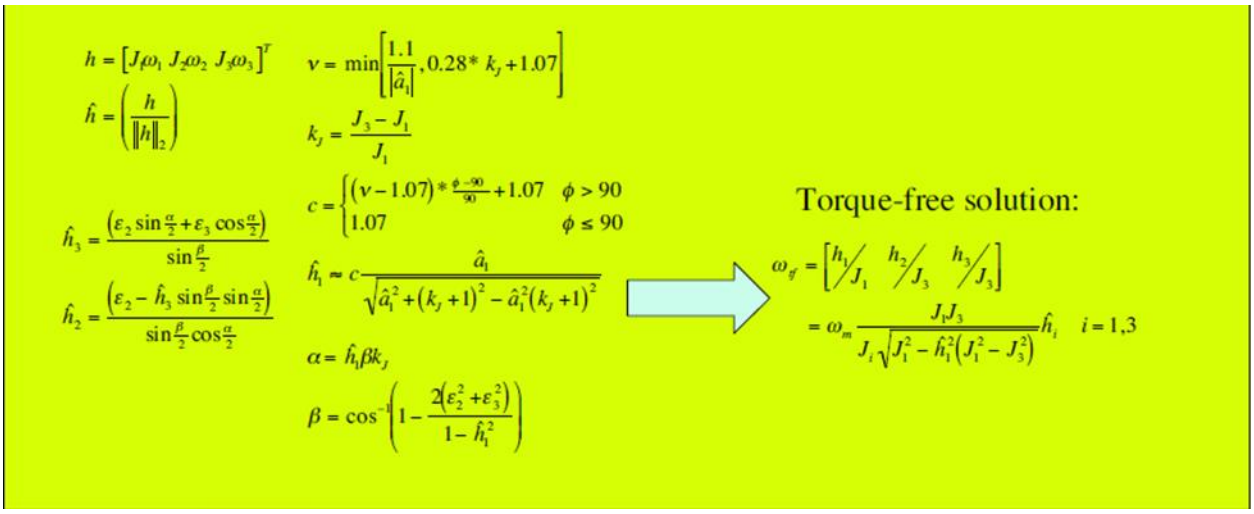

Figure 27. Approximate Solution to the Commanded Maneuver Rates to Follow a Torque Free Trajectory for vehicles with an axis of symmetry. See Reference [30]

RCS Maneuvers Using Steering Formulations

An alternative implementation for RCS rotational maneuvering is to implement steering logic typically found in closed-loop guidance algorithms. This implementation can avoid a large "step" in the initial attitude and rate errors when the maneuver is commanded. Avoiding this step in the attitude and rate commands can minimize overshoot/undershoot of the desired trajectory, however it may also increase RCS duty cycles due to the finer tracking of a ramped (as opposed to step) rate command. The formulation here follows closely from Reference [29] using a control law of the form:

$$\alpha_c + 2\zeta\omega_n\omega_e + \omega_n^2\phi_e = 0 \qquad \textbf{(11)}$$

Where:
α_c is the angular acceleration command,
ϕ_e is the attitude error, and
ω_e is the rate error, (the derivative of ϕ_e)
ζ, ω_n are gains of the control law.

Constraints on the maximum commanded acceleration and angular velocity (α_{max} and ω_{max}) are defined, the former related to available RCS control authority and the latter the desired steady state maneuver rate. Given these constraints, the commanded trajectory is a time-minimum solution which generally defaults to a bang-off-bang eigenaxis trajectory. If $\zeta=\sqrt{1/2}$, it can be shown[29] that $\omega_n = \frac{\alpha_{max}}{\omega_{max}}e^{\pi/4}$, and the control law in equation (11) follows the form in equation (12). Once the commanded vehicle acceleration is computed, the commanded rate and attitude profiles are generated by integration.

$$\alpha_c = -\sqrt{2}\,\frac{\alpha_{max}}{\omega_{max}}e^{\pi/4}\omega_e - \left(\frac{\alpha_{max}}{\omega_{max}}e^{\pi/4}\right)^2\phi_e \qquad \textbf{(12)}$$

A comparison of the performance for the three previous trajectory algorithms is shown in Figure 28, including two different commanded maneuvers. In the first case (LEO Coast 1), the EUS vehicle is oriented in a Sun normal attitude prior to maneuvering to the commanded LVLH attitude resulting in a multi-axis maneuver for which the torque-free rotation performs best in terms of propellant usage. In comparison, the resulting maneuver in the second case (LEO Coast 2), in which the vehicle is initially oriented in a tail-to-Sun attitude before maneuvering to the commanded LVLH attitude, is a multi-axis maneuver at constant rates and performs best when the eigenaxis rotation logic is used.

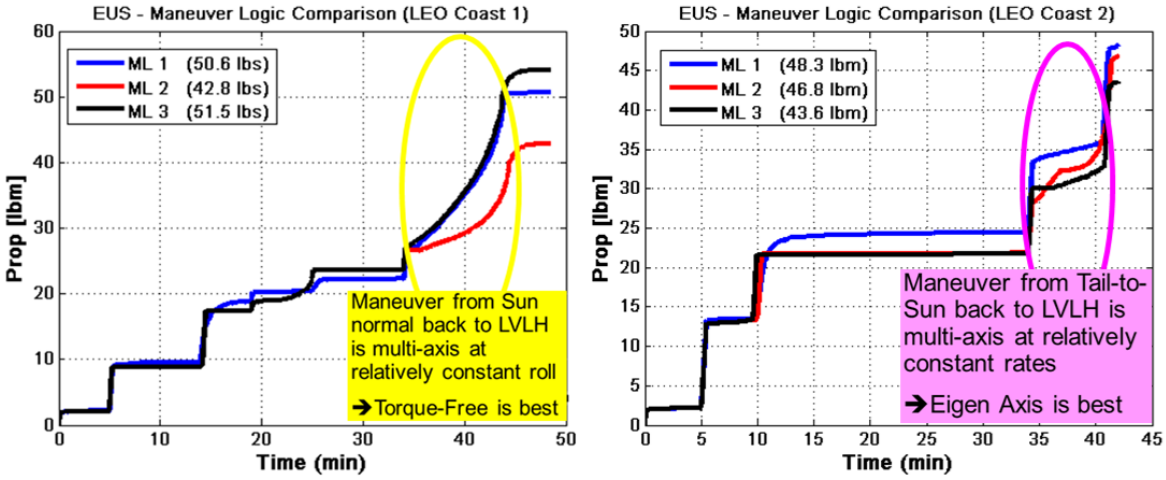

Figure 28. Vehicle Control Performance Results for Different Maneuver Algorithms (ML1: Steering Formulations, ML2: Torque-Free Trajectory, ML3: Eigenaxis Trajectory)

More Complex RCS Maneuvering Trajectories

More complex algorithms are available which better utilize initial conditions by using more than two pulses[30]. A full optimal trajectory solution[31] which considers other environmental disturbances (gravity gradient, aerodynamic, etc) using pseudospectral optimization has been demonstrated. The latter can provide significant propellant savings. For space operations where the attitude timeline is pre-defined, specifically for rotations where the initial and final boundary conditions (i.e. initial/final attitude and rotation rates) are known, this latter fuel-optimal trajectory can be computed a priori and off-line.

VI. Thruster Hardware Specifications

RCS thruster configuration design for efficiency and controllability is well understood[32]. Given a single fault-tolerant design constraint is utilized, a trade can be performed showing that the implementation of duplicate thrusters can potentially be avoided at the cost of propellant usage. Depending on cost and mass implications either a duplicate thruster approach or a propellant impacting approach can prove viable. Provided a duplicate thruster approach to redundancy, a thruster failure can be accommodated by switching to a redundant string of thrusters with little or no impact to control authority or RCS propellant consumption. Alternatively, thrusters can be oriented and located such that full 3-axis control can still be achieved following a thruster failure without having a redundant string of thrusters. The cost of this approach is that thruster locations and orientations needed for this capability will likely not be propellant optimal under nominal operation and could have additional RCS propellant consumption impacts following a thruster failure. Basic thruster location and sizing assessments are interconnected and therefore generally lead to a torque-based requirement. In general, the thrusters should be located sufficiently far from the mass center of the

vehicle at all points in flight. The thruster size and number is then linked to the resulting moment arm, vehicle inertia, expected disturbance torques, and maneuvering requirements.

From a GN&C perspective, RCS hardware requirements can be specified based on minimum and maximum torque capability rather than a specific number of thrusters with specific locations and orientations. This allows hardware designers to design the system based on availability of hardware, available space on the vehicle, and other mechanical design considerations.

A Space Shuttle heritage criteria can be applied for defining acceptable control authority of an RCS system. This design criteria requires the control torque to exceed all known disturbance torques by a factor of two. From the rotational equations of motion (equation 1), this criteria is written as:

$$\hat{T}_C > 2 * \left[\max\left(-\hat{\omega}\, x\, \hat{J}\hat{\omega} \right) + \max\left(\hat{T}_{ext} \right) \right]$$

where T_c is the required control torque, ω is the body rate, J is he inertia tensor, and T_{ext} is the summation of external disturbance torques. Worst case values are computed for each term and summed together to generate a peak disturbance value. Note the gyroscopic coupling effect from the Euler equations of motion is included and is a function of the desired rotational maneuver rate, meaning (obviously) if higher maneuver rates are desired, larger control authority is required. Disturbances to consider are generally a function of the orbit and attitude. For low Earth orbits, gravity gradient is often the primary environmental disturbance torque. Time domain simulation is used to demonstrate controllability of the vehicle with an RCS. The time domain simulation should have sufficient fidelity to model vehicle dynamics, expected maneuvers, and known disturbances. If the control authority of the RCS is marginal, the commanded vehicle maneuver rates can be reduced so as to reduce the gyroscopic effect.

While control authority is the primary concern for making sure the RCS is sized large enough, the design must also be assessed to ensure the desired control precision can be achieved. Control precision is impacted by both thruster force and minimum thruster on-time. Trades can be assessed based on pointing accuracy and the resulting duty cycle to ensure that the fine control of the vehicle is sufficient. System delays and latency are important when assessing time domain results for such purposes. If control accelerations are too great, propellant usage and limit cycling can be adversely impacted. Figure 29 shows an example of this sensitivity to key parameters. These results are based on time domain simulation using the same number of thrusters in the same locations/orientations but varying the thruster force magnitude. These results were generated for both a nominal and failed thruster scenario and show an optimal thruster size based on total impulse and therefore RCS propellant usage. It is also worth noting that for lower thrust jets, the On/Off count rises significantly. However, adding hysteresis to the phase plane design can reduce this effect as shown in the figure.

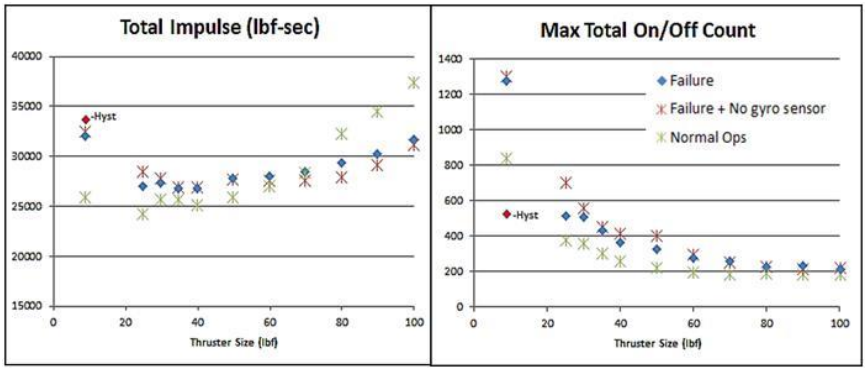

Figure 29. Time Domain Simulation Showing Sensitivity of Total Thruster Impulse and On/Off Count to Thruster Force Size

VII. Summary

A summary of key principles for the design and stability determination of a spacecraft on-orbit attitude control system employing constant-thrust on-off Reaction Control System (RCS) thrusters has been presented. Drawing from Space Shuttle and Space Station program experience and using advancements made in support of the initial development of the NASA Exploration Upper Stage vehicle, insight and design principles for control system hardware performance requirements, control system software algorithms, and software filter design have been provided. Topics addressed included thruster hardware specification, phase plane design and stability, jet selection approaches, filter design metrics, and auto maneuver logic. An approach using Describing Functions to linearize a system modeling a nonlinear phase plane algorithm has been described in detail, and consistency of this approach with time domain nonlinear simulation has been demonstrated.

VIII. Acknowledgments

This work was completed at the NASA Marshall Space Flight Center in support of Space Launch System development under the Jacobs Engineering ESSSA contract. Much of this work draws from research and development performed by the Charles Stark Draper Laboratory in its support of the Space Shuttle and International Space Station Programs. Special thanks to Paul Van der Porten/MSFC and Logan Kennedy/MSFC for their expertise and support related to guidance and control.

IX. References

[1] Hughes, P. C., *Spacecraft Attitude Dynamics*, John Riley and Sons, New York, 1986.
[2] Bryson, A. E. Jr., *Control of Spacecraft and Aircraft*, Princeton University Press, Princeton, New Jersey, 1991.
[3] Kubiak, E., "Phase Plane Logic Design Principles", NASA Johnson Space Center Memorandum, EH2-86M-149, May 30, 1986.
[4] Widnall, W. S., "Lunar Module Digital Autopilot", *Journal of Spacecraft and Rockets*, Vol. 8, No. 1 (1971), pp. 56-62.
[5] Zimpfer, D., Kirchway, C., Hanson, D., Jackson, M., Smith, N., "Shuttle Stability and Control of the STS-71 Shuttle/MIR Mated Configuration", AAS/AIAA Space Flight Mechanics Meeting, Austin, Texas, February 1996, AAS-96-131.
[6] "Space Shuttle Orbiter Operational Level C Functional Subsystem Software Requirements (FSSR) Guidance Navigation and Control Part C, Flight Control Orbit DAP", Prepared by the Boeing Company, STS-83-0009-30, December 14, 2000.
[7] Wie, B., *Space Vehicle Dynamics and Control*, AIAA Educational Series, American Institute of Aeronautics and Astronautics, Inc., Reston Virginia, 1998.
[8] Orr, J. S., Wall, J. H., VanZwieten, T. S., Hall, C. E., "Space Launch System Ascent Flight Control Design", 2014 American Astronautical Society (AAS) Guidance, Navigation, and Control Conference; Jan.-Feb. 2014; Breckenridge, Colorado, AAS 14-038.
[9] Jang, J., Plummer, M., Bedrossian, N., Hall, C., Jackson, M., Spanos, P., "Absolute Stability Analysis of a Phase Plane Controller Spacecraft", 20th AAS/AIAS Space Flight Mechanics Meeting, San Diego, California, February 2010, AAS-10-112.
[10] Penchuck, A., Hattis, P., Kubiak, E., "A frequency Domain Stability Analysis for a Phase Plane Control System", *Journal of Guidance, Control, and Dynamics*, Vol. 8, No. 1, 1985, pp. 50-55.
[11] Elgersma, M., Stein. G., Jackson, M., Matulenko, R. Caldwell, B., "*Space Station Attitude Control Using Reaction Control Jets*", Proceeding of the 31st Conference on Decision and Control, IEEE, Tucson, Arizona, December 1992, WM6-14:20.
[12] Plummer, M., "Stability Analysis of a Phase Plane Control System", Rice University Master of Science Thesis, Houston, Texas, 2009.
[13] Gelb, A., Vander Velde, W., E., *Multi-Input Describing Functions and Nonlinear System Design*, McGraw-Hill Book Company, New York, 1968.
[14] Hall, R., Barrington, R., Kirchwey, K., Alaniz, A., Grigoriadis, K., "Shuttle Stability and Control During the Orbiter Repair Maneuver", AIAA Guidance, Navigation, and Control Conference, August 2005, San Francisco, California, AIAA 2005-5852.
[15] Hamelin, J., L., Jackson, M., C., Kirchwey, C., B., Pileggi, R., A., "STS-99 Shuttle Radar Togography Mission Stability and Control", AAS/AISS Conference, Quebec City, Canada, August 2001, AAS-01-347.
[16] Jackson, M., Zimpfer, D., Lepanto, J., "Identification of Shuttle/MIR Structural Dynamics for Notch Filter Tuning", AAS/AIAA Space Flight Mechanics Meeting, Austin, Texas, February 1996, AAS-96-132.
[17] Hall, R., "Orbiter Minimum Angle Jet Select", AIAA Technical Symposium, Houston Texas, May 1993.
[18] Bergmann, E., V., Croopnick, S., R., Turkovich, J., J., Work, C., C., "An Advanced Spacecraft Autopilot Concept", Journal of Guidance, Control, and Dynamics, May-June 1979, Vol 2. No 3. Article No. 77-1071.
[19] Glandorf, D., Martin, M., "Optimal Jet Selection for Spacecraft", AIAA Technical Symposium, Houston, Texas, May 10, 1985.
[20] Kubiak, E., Davison, R., "A Phase Plane Logic Design to Interface with "Optimal"-Type Jet Selection Algorithms", NASA Johnson Space Center EH2-86L-001, July 14, 1985.
[21] Singhose, W., E., Banerjee, A., K., Seering, W. P., "Slewing Flexible Spacecraft with Deflection-Limiting Input Shaping", Journal of Guidance, Control, and Dynamics, Vol. 20 No 2, March-April 1997.

[22] Bedrossian, N., S., Lepanto, J., A., Adams, N., Sunkel, J., Hua, T., "Jet Firing Strategy to Minimize Structural Loads*", Proc. 1995 American Control Conferenc*e, pp. 3622-3626 vol 5.
[23] Ickes, B. P., "A New Method for Performing Digital Control System Attitude Computations Using Quaternions", *AIAA Journal*, Vol. 8, No. 1, January 1970.
[24] Redding, D., C., Adams, N. J., "Optimized Rotation Axis Attitude Maneuver Controller for the Space Shuttle Orbiter", *Journal of Guidance, Control, and Dynamics*, Vol. 10, No. 1, p. 4, 1987.
[25] Dixon, M., V., Edelbaum, T., N., Potter, J., E., Vandervelde, W., E., "Fuel Optimal Reorientation of Axisymmetric Spacecraft", *Journal of Spacecraft and Rockets*, Vol. 7, No. 1, November 1970.
[26] Kaznacheyev, Branets, Chertok, "Optimal Turning of Rigid Body with One Symmetry Axis", translation from Kosmicheskie Issledovaniya, Vol 22, No. 3, May-June 1984.
[27] Hall, R. A., Kaznacheyev, Y., V., "Fuel Optimal Rotations of the Space Station MIR", AIAA Guidance, Navigation, and Control Conference, San Diego, California, July 1996, AIAA 96-3789.
[28] Hall, R. A., Lowry, N., C., "Cost functions for Bang-Off-Bang Control of Axisymmetric Spacecraft", *Advances in the Astronautical Sciences*, AAS Spaceflight Mechanics 2003 Proc., vol 1. pp 45-53, AAS 03-102.
[29] Henry, R. L., Brand, T. J., Long, A.D., Cockrell, B.F., Thibodeau III, J.R., "Space Shuttle Ascent Guidance, Navigation, and Control", State of the Art Paper, Journal of the Astronautical Sciences, Vol XXVII, No 1, pp 1-38, January-March, 1979.
[30] Hall, R., A., Lowry, N., C., Ghorbel, F., "Three-Pulse Reduced Fuel Rotations of Axisymmetric Spacecraft Using Reaction Control Thrusters", ACC03-AIAA-0067, American Control Conference, August 2003.
[31] Bhatt, S., Bedrossian, N., Longacre, K., Nguyen, L., "Optimal Propellant Maneuver Flight Demonstrations on ISS", AIAA Guidance, Navigation, and Control Conference, Boston, Massachusetts, August 2013.
[32] Crawford, B., S., "Configuration Design and Efficient Operation of Redundant Multi-Jet Systems", AIAA Guidance, Control, and Flight Mechanics Conference, Princeton, New Jersey, August 1969, No. 69-845.